Deficiency of the aryl hydrocarbon receptor in intestinal epithelial cells, but not hepatocytes, ameliorates atherosclerosis development by sex-dependently targeting the lipid metabolism

Rosanna Huchzermeier[1,2,3], Leonida Rakateli[1,2], Melissa Corcini-Berndt[1,2,3], Sanne L. Maas[1,2,3], Kathrin Abschlag[1,2,3], Chantal Maassen Pöttgens[1,2,3], Julia Moellmann[1], Tabea Pirker[1], Susanne Kremer[4], Julia Steitz[4], Han Jin[5,6], Boyu Ji[7], Stefan Düsterhöft[8], Caspar Ohnmacht[9], Renske J. de Jong[10], Emiel P.C. van der Vorst[1,2,3,11]

Supplementary material – Table of contents

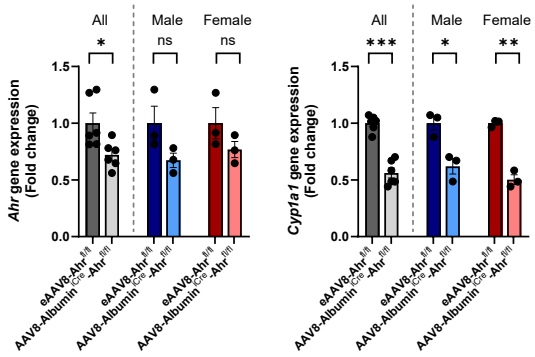

Supplementary Figure 1. Knockout validation in *AAV8-Albumin^{iCre}-Ahr$^{fl/fl}$* and *eAAV8-Ahr$^{fl/fl}$* mice.

x-fold mRNA expression in the liver of *AAV8-Albumin^{iCre}-Ahr$^{fl/fl}$* and *eAAV8-Ahr$^{fl/fl}$* mice reflecting *Ahr* expression and expression of one of its main target genes *Cyp1a1*. Graphs represent mean ± SEM. Combined n=6, male n=3, female n=3. **P*<0.05, ***P*<0.01, ****P*<0.001.

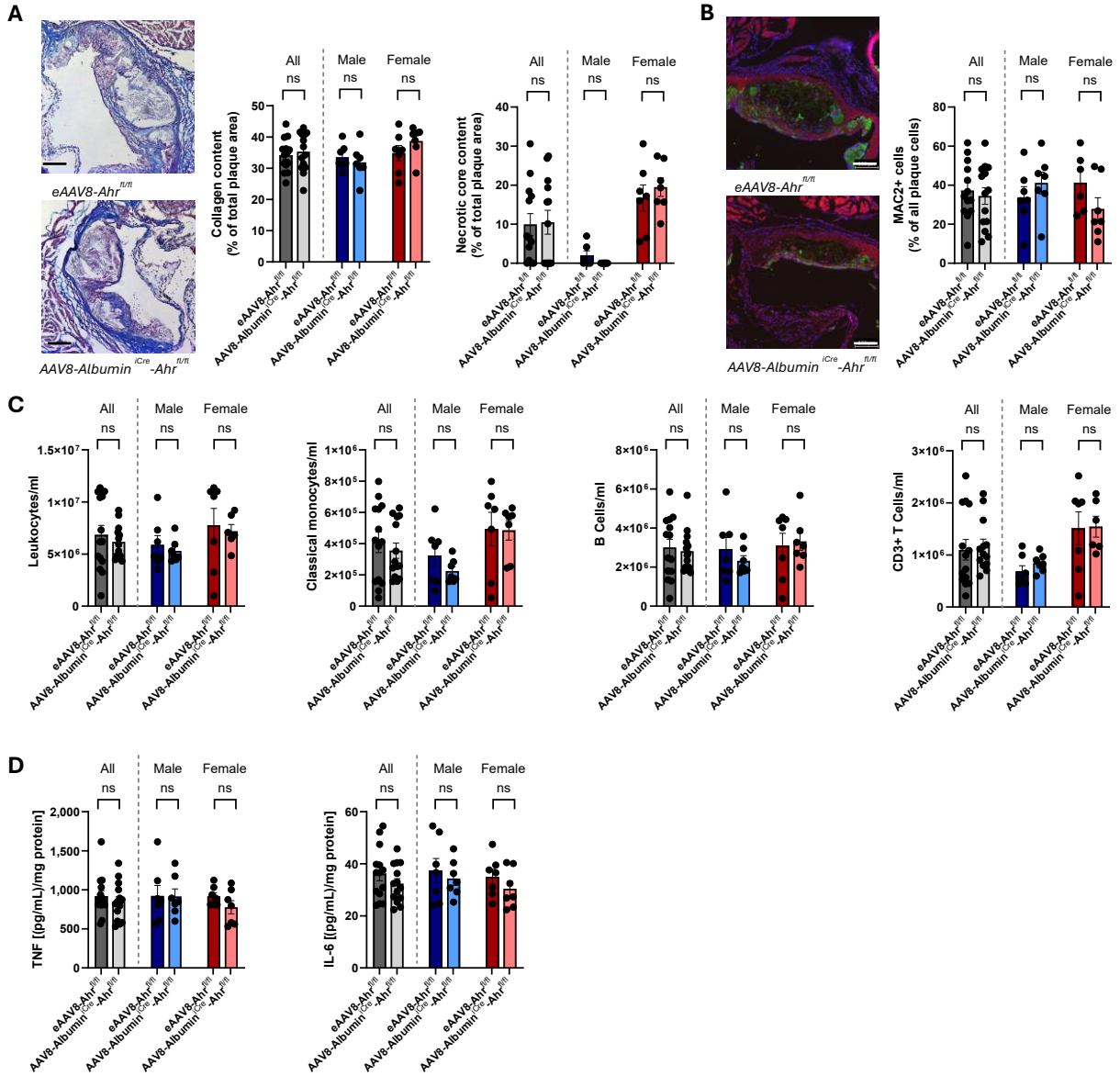

Supplementary Figure 2. Detailed characterization of *AAV8-Albumin^{iCre}-Ahr$^{fl/fl}$* and *eAAV8-Ahr$^{fl/fl}$* mice. *AAV8-Albumin^{iCre}-Ahr$^{fl/fl}$* and *eAAV8-Ahr$^{fl/fl}$* mice were fed a HFD for 12 weeks. **(A)** Representative pictures of Masson trichrome-stained aortic roots (scale = 100µm) and quantification of collagen content (Combined n=14, male n=7, female n=7) and necrotic core content (Combined n=13, male n=6, female n=7). **(B)** Representative pictures of MAC2+ stained aortic roots (scale = 100µm) and quantification of MAC2+ cells as a percentage of all DAPI+ plaque cells (Combined n=13 (*eAAV8-Ahr$^{fl/fl}$*) or n=14 (*AAV8-Albumin^{iCre}-Ahr$^{fl/fl}$*), male n=7, female n=6 (*eAAV8-Ahr$^{fl/fl}$*) or n=7 (*AAV8-Albumin^{iCre}-Ahr$^{fl/fl}$*)). **(C)** Blood total leukocyte and leukocyte subset counts (Combined n=14, male n=7, female n=7). **(D)** TNF and IL-6 levels in the liver (Combined n=14, male n=7, female n=7). Graphs represent mean ± SEM.

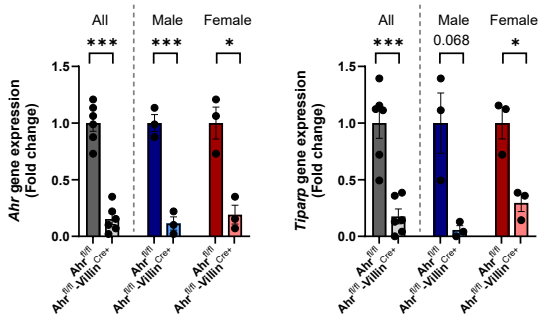

Supplementary Figure 3. Knockout validation in *Ahr*$^{fl/fl}$ *Villin*$^{Cre+}$ and *Ahr*$^{fl/fl}$ mice.

x-fold mRNA expression in the intestine of *Ahr*$^{fl/fl}$ *Villin*$^{Cre+}$ and *Ahr*$^{fl/fl}$ mice reflecting *Ahr* expression and expression of one of its main target genes *Tiparp*. Graphs represent mean ± SEM. Combined n=6, male n=3, female n=3. **P*<0.05, ****P*<0.001.

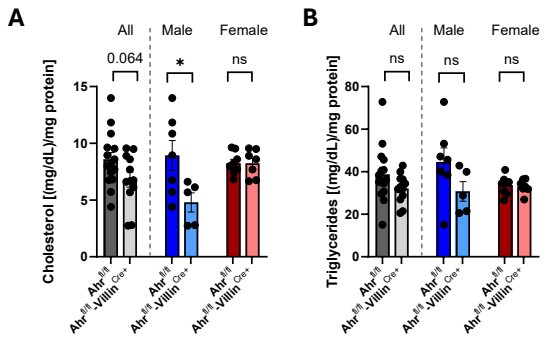

Supplementary Figure 4. Liver lipids in *Ahr*$^{fl/fl}$ *Villin*$^{Cre+}$ and *Ahr*$^{fl/fl}$ mice.

(A-B) Liver cholesterol (A) and liver triglyceride (B) in Ahr$^{fl/fl}$ Villin^{Cre+} and Ahr$^{fl/fl}$ mice after a 12-week HFD. Graphs represent mean ± SEM. Combined n=15 (*Ahr*$^{fl/fl}$) or n=12 (*Ahr*$^{fl/fl}$*Villin*$^{Cre+}$), male n=7 (*Ahr*$^{fl/fl}$) or n=5 (*Ahr*$^{fl/fl}$*Villin*$^{Cre+}$), female n=8 (*Ahr*$^{fl/fl}$) or n=7 (*Ahr*$^{fl/fl}$*Villin*$^{Cre+}$). *P<0.05.

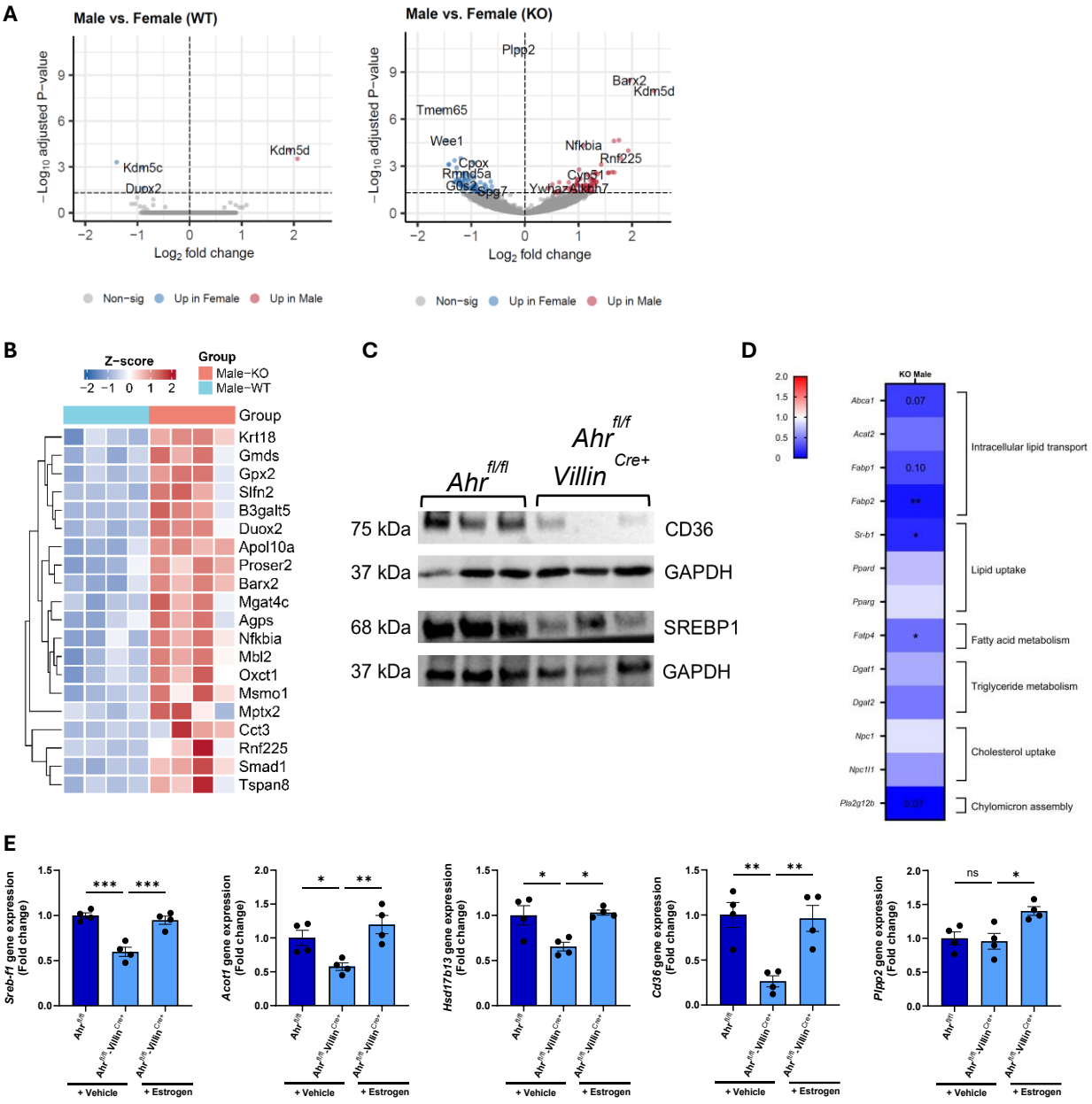

Supplementary Figure 5. Modified gene and protein expression in the duodenum of *Ahr*$^{fl/fl}$ *Villin*$^{Cre+}$ and *Ahr*$^{fl/fl}$ mice.

(**A**) Volcano plots of differentially regulated genes determined with RNA sequencing in the duodenum of *Ahr*$^{fl/fl}$ (WT; n=4 per sex) and *Ahr*$^{fl/fl}$ *Villin*$^{Cre+}$ (KO; n=4 per sex) comparing male vs. female after a 12-week HFD. (**B**)Top 20 upregulated genes in the duodenum of male mice after a 12w HFD. n=4 per sex. (**C**) Western Blot analysis of duodenum lysates of male *Ahr*$^{fl/fl}$ *Villin*$^{Cre+}$ and *Ahr*$^{fl/fl}$ mice after a 12w HFD (n=3). (**D**) x-fold mRNA expression in the duodenum of male *Ahr*$^{fl/fl}$ *Villin*$^{Cre+}$ *vs. Ahr*$^{fl/fl}$ mice after a 12w HFD of lipid-metabolism-related genes. *P* values are indicated in the graph as a number or as an asterisk. n=5. (**E**) Relative mRNA expression of small intestinal epithelial organoids derived from males. *Ahr*$^{fl/fl}$ or *Ahr*$^{fl/fl}$ *Villin*$^{Cre+}$ mice on a standard laboratory diet treated with estrogen or v/v ethanol as vehicle control (n=4). The relative mRNA expression was calculated as fold changed compared to vehicle control treated *Ahr*$^{fl/fl}$ mice. Graphs represent mean ± SEM. **P*<0.05.

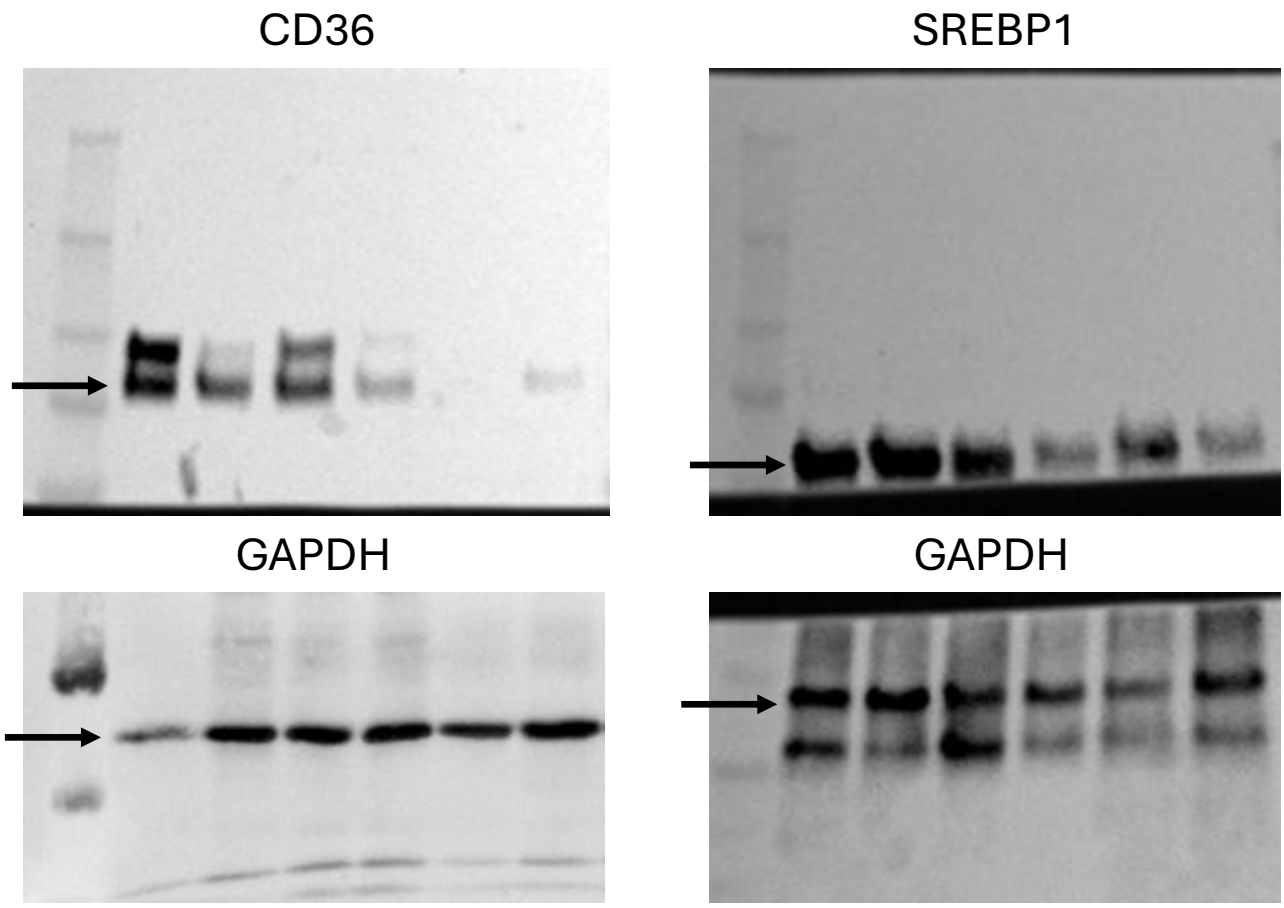

Supplementary Figure 6. Uncropped Western blots of Figure 5C.

Western Blot analysis of duodenum lysates of male *Ahr*$^{fl/fl}$ *Villin*$^{Cre+}$ and *Ahr*$^{fl/fl}$ mice after a 12w HFD. Arrows indicate the bands shown in Figure 5C.

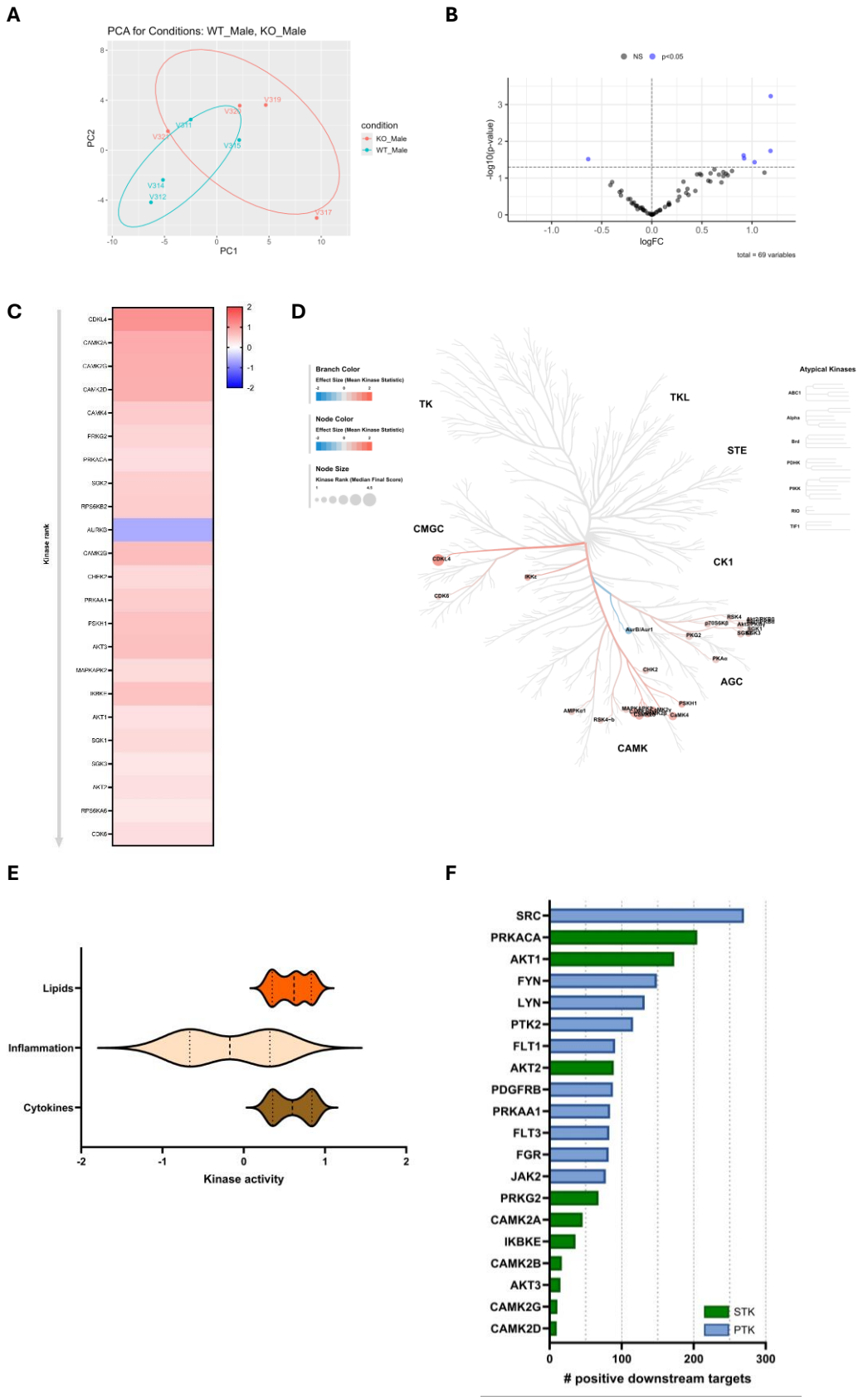

Supplementary Figure 7. Kinase profiling of intestinal tissue of male mice.

(A-F) Kinase profiling on intestinal lysates from male *Ahr*$^{fl/fl}$ *Villin*$^{Cre+}$ compared to Ahr$^{fl/fl}$ mice after a 12-week HFD. **(A)** Principal component analysis (PCA) depicting the variance in STK-related peptide phosphorylation

profiles. **(B)** Volcano plot displaying differentially phosphorylated STK-related peptides. Blue dots represent significant differential phosphorylation of peptides between the two groups ($P < 0.05$). Total variables denote the number of peptides with measurable phosphorylation levels. **(C)** Heatmap showing effect size (mean kinase statistic) for STKs, sorted based on kinase rank (mean kinase score). Blue reflects downregulated activity, while red reflects upregulated activity in intestines from $Ahr^{fl/fl}$ $Villin^{Cre+}$ compared to $Ahr^{fl/fl}$ mice, respectively. **(D)** Kinome coral tree depicting kinase rank (node size) and the effect size (node and branch color) of significantly differentially regulated kinases. **(E)** Kinase activity of STKs involved in the selected pathway clusters, based on mean kinase statistic. Negative value reflects reduced activity in intestines from $Ahr^{fl/fl}$ $Villin^{Cre+}$ compared to $Ahr^{fl/fl}$ mice. **(F)** Number of positively regulated direct downstream substrates/targets for each kinase involved in regulated lipid pathways. n=4 per sex.

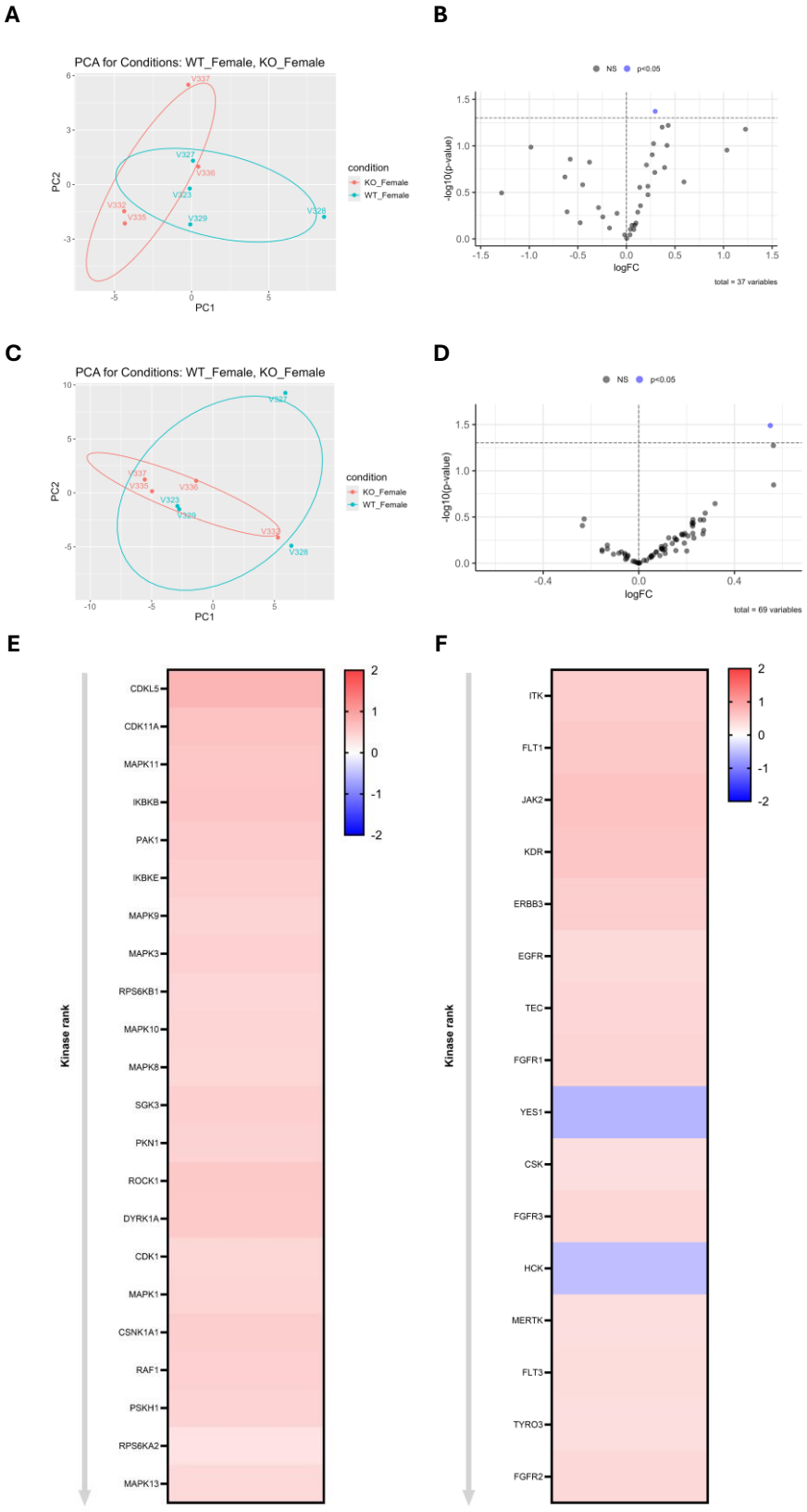

Supplementary Figure 8. Kinase profiling of intestinal tissue of female mice.

(A-F) Kinase profiling on intestinal lysates from female *Ahr*$^{fl/fl}$ *Villin*$^{Cre+}$ compared to Ahr$^{fl/fl}$ mice after a 12-week HFD. **(A)** Principal component analysis (PCA) depicting the variance in PTK-related peptide phosphorylation profiles. **(B)** Volcano plot displaying differentially phosphorylated PTK-related peptides. Blue dots represent

significant differential phosphorylation of peptides between the two groups ($P < 0.05$). Total variables denote the number of peptides with measurable phosphorylation levels. **(C)** Principal component analysis (PCA) depicting the variance in STK-related peptide phosphorylation profiles. **(D)** Volcano plot displaying differentially phosphorylated STK-related peptides. Blue dots represent significant differential phosphorylation of peptides between the two groups ($P < 0.05$). Total variables denote the number of peptides with measurable phosphorylation levels. **(E)** Heatmap showing effect size (mean kinase statistic) for PTKs, sorted based on kinase rank (mean kinase score). Blue reflects downregulated activity, while red reflects upregulated activity in intestines from $Ahr^{fl/fl}$ $Villin^{Cre+}$ compared to $Ahr^{fl/fl}$ mice, respectively. **(F)** Heatmap showing effect size (mean kinase statistic) for STKs, sorted based on kinase rank (mean kinase score). Blue reflects downregulated activity, while red reflects upregulated activity in intestines from $Ahr^{fl/fl}$ $Villin^{Cre+}$ compared to $Ahr^{fl/fl}$ mice, respectively. n=4 per sex.

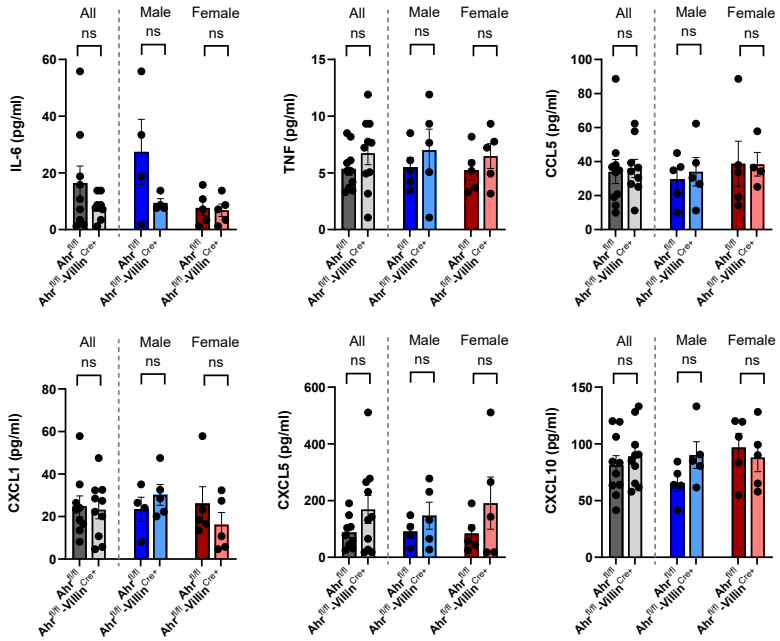

Supplementary Figure 9. Inflammatory profile of *Ahr*$^{fl/fl}$ *Villin*$^{Cre+}$ and *Ahr*$^{fl/fl}$ mice.

Plasma cytokine levels measured by Multiplex analysis. Graphs represent mean ± SEM. Combined n=10, male n=5, female n=5.